NASA TECHNICAL NOTE

NASA TN D-8034

4.

VORTEX SHEDDING FROM A BLUNT TRAILING EDGE WITH EQUAL AND UNEQUAL EXTERNAL MEAN VELOCITIES

Paul F. Brinich, Donald R. Boldman, and Marvin E. Goldstein

Lewis Research Center
Cleveland, Ohio 44135

3. NATIONAL AERONAUTICS AND SPACE ADMINISTRATION • WASHINGTON, D. C. • AUGUST 1975

5.

1. Report No.	2. Government Accession No.	3. Recipient's Catalog No.
NASA TN D-8034		

4. Title and Subtitle
VORTEX SHEDDING FROM A BLUNT TRAILING EDGE WITH EQUAL AND UNEQUAL EXTERNAL MEAN VELOCITIES

5. Report Date
August 1975

6. Performing Organization Code

7. Author(s)
Paul F. Brinich, Donald R. Boldman, and Marvin E. Goldstein

8. Performing Organization Report No.
E-8281

10. Work Unit No.
505-03

9. Performing Organization Name and Address
Lewis Research Center
National Aeronautics and Space Administration
Cleveland, Ohio 44135

11. Contract or Grant No.

13. Type of Report and Period Covered
Technical Note

12. Sponsoring Agency Name and Address
National Aeronautics and Space Administration
Washington, D.C. 20546

14. Sponsoring Agency Code

15. Supplementary Notes

16. Abstract

A flow visualization study has shown that strong Karman vortices are developed behind the blunt trailing edge of a plate when the free stream velocities over both surfaces are equal. These vortices tend to disappear when the surface velocities are unequal. This observation provided an explanation for the occurrence and disappearance of the lip noise often present in coaxial jets. Vortex formation and lip noise occurred at a Strouhal number of about 0.2 based on the lip thickness and the average of the external steady-state velocities. Results from theoretical calculations of the vortex formation, based on an inviscid, incompressible analysis of the motion of point vortices, were in good agreement with the experimental observations.

17. Key Words (Suggested by Author(s))
Fluid mechanics
Incompressible flow
Wakes
Vortices

18. Distribution Statement
Unclassified - unlimited
STAR Category 34 (rev.)

19. Security Classif. (of this report)	20. Security Classif. (of this page)	21. No. of Pages	22. Price*
Unclassified	Unclassified	29	$3.75

* For sale by the National Technical Information Service, Springfield, Virginia 22161

VORTEX SHEDDING FROM A BLUNT TRAILING EDGE WITH EQUAL AND UNEQUAL EXTERNAL MEAN VELOCITIES

by Paul F. Brinich, Donald R. Boldman, and Marvin E. Goldstein

Lewis Research Center

SUMMARY

A flow visualization study has shown that strong Karman vortices are developed behind the blunt trailing edge of a plate when the free stream velocities over both surfaces are equal. These vortices tend to disappear when the surface velocities are unequal. This observation provided an explanation for the occurrence and disappearance of the lip noise often present in coaxial jets. Vortex formation and lip noise occurred at a Strouhal number of about 0.2 based on the lip thickness and the average of the external steady-state velocities.

Results from theoretical calculations of the vortex formation, based on an inviscid, incompressible analysis of the motion of point vortices, were in good agreement with the experimental observations.

INTRODUCTION

In the study of subsonic jet noise it has been found that the noise produced by a coaxial jet has certain peculiarities which depend on the ratio of the primary to secondary jet velocities (refs. 1 and 2). The dependency is most easily described by referring to figure 1 where the power level noise spectra for a coaxial nozzle are shown for various ratios of secondary to primary air velocity. The feature of interest to the present investigation is the spike of narrow band high frequency noise that occurs at the higher velocity ratios and which decreases as the velocity ratio is reduced. The noise finally disappears into the jet broad band noise at velocity ratios below 0.5. The Strouhal number for this narrow band noise based on the thickness of the lip separating the two streams is approximately 0.2, which suggests the presence of a Karman vortex street emanating from this lip.

The purpose of this investigation therefore was to study the flow in the wake region of a blunt trailing edge, particularly as it relates to the Karman vortex street generation, having either equal or unequal velocities over the top and bottom surfaces of a flat plate. Such a flow is believed to be a reasonable simulation of the interaction between coaxial jets. Further, it is hoped to establish a rational explanation of the observed lip noise phenomena based on established fluid-mechanical behavior. Although the primary air flow in the noise experiments described by reference 1 was 244 m/sec, the velocities in the present experiment were reduced by a factor of 10 in order to use smoke visualization techniques to study the vortex development in the wake. However, the Reynolds number was approximately the same in the two cases.

SYMBOLS

A, B	disturbance amplitude constants
a	disturbance wavelength
f	frequency
h	vertical distance between vortex rows or thickness of trailing edge
N	number of point vortices in each vortex sheet
St	Strouhal number
t	time
U	free stream velocity
$\overline{U}$	average free stream velocity, $(U_1 + U_2)/2$
U_r	ratio of free stream velocity, U_2/U_1
u	local mean velocity induced x-component velocity for each point vortex
u'	rms value of x-component of fluctuating velocity
V	x-component of cloud velocity
v	induced y-component velocity for each point vortex
x	distance in stream direction
y	distance perpendicular to vortex sheet
δ	boundary layer thickness at point where velocity ratio is 0.99

Subscripts:

j	identification of point vortex

k identification of point vortex

1 refers to upper velocity

2 refers to lower velocity

Superscripts:

+ refers to upper vortex row

- refers to lower vortex row

APPARATUS AND INSTRUMENTATION

The Karman vortex street was produced downstream of the blunt trailing edge of the flat plate installed in the 9.8- by 25.4-cm wind tunnel as indicated in figure 2. The flat plate model was 79 cm long (excluding the faired leading edge which extended forward 2.5 cm), 9.8 cm wide, and 1.3 cm thick. The width of the forward half of the plate was contoured to fit the entrance bell mouth, and it was this part that served to attach the plate to the tunnel structure. The downstream half of the plate was supported between the glass walls of the tunnel by friction. Elastic seals between the plate and the tunnel walls prevented leakage of air from the top to the bottom of the plate.

A single layer of steel window screening (18 mesh; 7 wires per cm) was sandwiched between the steel bellmouth flange and the wood fairing, likewise between the forward edge of the plate and the leading edge fairing. This screening served to hold the various layers of cloth which were placed on the lower half of the inlet to vary the velocity ratio of the flow over the lower surface to that over the upper surface between zero and unity.

Instrumentation on the flat plate model consisted of two static pressure taps 2.5 and 22.9 cm upstream of the trailing edge along the centerline on the top of the plate and two similarly placed taps on the lower surface of the plate. Upper and lower tunnel wall static pressure taps were in line with the plate static pressure taps. An additional static pressure tap was located on the blunt base. Two pitot tubes were installed along the centerline of the plate 20.3 cm downstream of the screen on the upper and lower surfaces as shown in figure 2. A 0.76-cm-inside-diameter tube extended the full length of the model and was used to supply smoke for visualization of the flow in the wake region. The center of this tube was offset 0.76 cm from the spanwise centerline of the model and the base static pressure tap was offset an equal amount on the other side of the model centerline. The smoke tube and the model pressure instrumentation leads extended straight ahead of the leading edge 30 cm before making a lateral turn toward the smoke generator and the manometer.

The smoke was generated by burning cigars in an apparatus similar to that described by Herzig, Hansen, and Costello (ref. 3) except that the cigars were not soaked

in oil as suggested in the reference. Instead, it was found that a cigar moistened with water provided a sufficiently dense smoke for photographic purposes. A 16-mm high-speed motion picture camera was used to photograph the flow in the base region. The camera was operated at about 2300 frames per second and covered a field of view of about 7.6 by 10.2 cm as shown in figure 2. The camera was directed to give a slightly oblique view of the trailing edge as indicated in the top view of figure 2 and the enlarged photograph at the top of figure 3.

Plate boundary layers were measured immediately upstream of the trailing edge using flattened boundary layer pitot tubes. Wake velocity and turbulent intensity profiles were measured at 2.5 and 7.6 cm downstream of the plate trailing edge using single-element hot wire probes. All of the aforementioned surveys were made along the plate centerline.

In order to be assured of a turbulent boundary layer over the plate, a strip of No. 180 abrasive paper 5.7 cm long and spanning the width of the plate was attached to the upper and lower surfaces of the plate 28 cm upstream of the trailing edge.

EXPERIMENTAL RESULTS

The experiment was performed at essentially one free stream velocity $U_1 = 24.4$ m/sec, over the upper surface of the plate and at several velocities U_2 on the lower surface to give ratios of lower to upper velocity of 0, 0.25, 0.50, 0.75, and 1.0. The stream velocity of 24.4 m/sec represents an upper limit to visualization of the vortex cloud smoke patterns. At lower velocities the vortex cloud smoke patterns became more distinct, but difficulty in throttling the airstream precluded operation at the lower levels. To the unaided eye the smoke pattern behind the trailing edge resembled a steady wake flow. Use of a stroboscopic light did not change matters much - vortex cloud patterns still could not be seen. However, use of a high-speed motion picture camera operating at 2300 frames per second revealed the vortex shedding in sufficient detail so that shedding frequency, vortex cloud velocity, and wake divergence could be estimated fairly well.

Figures 3(a), (b), (c), (d), and (e) are enlargements (twice regular size) of selected motion picture frames which show some of the differences that occur as the velocity ratio is changed from unity to zero. To clarify these pictures for the viewer, a 6 times enlarged, slightly retouched photograph is presented at the top of figure 3 which indicates more clearly what the motion picture frames represent. It is generally conceded that a single or even a collection of single frames from high-speed motion pictures of a periodic phenomena is an inadequate substitute for the film viewed with a good movie projector, since the lack of clarity in a single frame is compensated by the advantage of

being able to detect motion. Another problem is that there may be no typical frame or frames, that is, the phenomenon may not be steady over long periods of time. Thus, in some of the present movie films a well-defined vortex cloud pattern may exist for a while and at another time be relatively poorly defined. Bearing these considerations in mind, the descriptions of the vortex shedding which follow should be regarded as more or less typical.

When the velocity ratio was unity (fig. 3(a)), a sequence of well-defined vortex clouds was shed from the top and bottom edge of the plate in such a way that a bottom cloud was positioned midway between two top clouds and vice versa. This is the classical vortex shedding phenomenon known as the Karman vortex street which is known to occur in the Reynolds number range from 300 to 10^5 for turbulent flow (ref. 4). The Reynolds number of the present study based on the trailing edge thickness and the upper air velocity was 2×10^4. The wake total divergence angle measured on a movie screen was about 20°, the vortex shedding rate was about 370 Hz, and the vortex velocity was around 17.4 m/sec. Both the upper and lower vortex clouds appeared to be of equal strength.

Figure 3(b) shows a sequence taken when the velocity ratio was 0.75 (the flow over the lower surface was reduced). The predominant change in this picture is that the bottom vortex clouds are no longer midway between the top clouds, but tend to be overtaken by the upper ones and are more poorly defined. The shedding rate of the upper clouds is reduced to 325 Hz, the vortex velocity is 14.6 m/sec, and the divergence angle remains at 20°. As the velocity ratio was reduced to 0.5 (fig. 3(c)) the shedding rate dropped to 315 Hz, the vortex velocity was about 15.2 m/sec, and the divergence angle of the wake reduced to 6°. For this condition the vortex clouds off the lower surface appeared much weaker and were overtaken very quickly by the upper ones.

At a velocity ratio of 0.25 (fig. 3(d)), only vortex clouds from the upper surface could be seen. These were shed at a rate of about 350 Hz and were very difficult to detect (hot wire measurements using a narrow band wave analyzer indicated no predominant shedding frequency). The vortex cloud velocity could not be estimated because the clouds were too indistinct. When the velocity ratio was reduced to zero (fig. 3(e)), vortices having a characteristic frequency could not be detected and the wake appeared as a succession of random eddies. For both the 0.25 and zero velocity ratios very little spreading of the wake took place in the region of observation.

Boundary layer velocity profiles measured immediately upstream of the trailing edge were typically turbulent for all the flow conditions down to a velocity ratio of 0.41. Figure 4 compares measured boundary layer velocity profiles at velocity ratios of 1.0 and 0.41 with the one-seventh power law commonly assumed for the turbulent boundary layer. The agreement between the power law and the measured profiles is good enough to conclude that the measured profiles are typically turbulent. Since boundary layer

profiles below the velocity ratio 0.41 were not measured, it cannot be definitely stated that they were turbulent. However, the Reynolds number based on plate length at a velocity ratio of 0.25 (velocity = 6 m/sec) along the lower surface is 3.2×10^5, which is near the lower limit for turbulent flow to exist (ref. 5). However, the presence of the sandpaper roughness upstream on the plate may be sufficient to ensure turbulent flow at this condition.

Hot wire surveys of the velocity and turbulent intensity in the wake region were obtained at $x = 2.5$ centimeters downstream of the trailing edge for velocity ratios of 1.0, 0.75, 0.5, 0.25, and 0 and at $x = 7.6$ centimeters for velocity ratios of 1.0, 0.75, 0.31, and 0. These profiles are shown in figures 5 and 6 and indicate a thinning of the wake as the velocity ratio is reduced, as evidenced by the steepening of the profile slopes. This thinning was noted in both the steady-state velocity profiles and the turbulent intensity profiles and agrees qualitatively with the wake thinning noted in the vortex street motion pictures mentioned earlier.

Shedding frequencies at a distance of 2.5 cm downstream of the trailing edge were also measured with the hot wire apparatus and a frequency analyzer. These results are compared with the results previously mentioned for the motion picture film in table I. Agreement is quite good between the hot wire measurements of shedding frequency and the results derived from the motion picture film. The observed trend of decreasing shedding frequencies at velocity ratios $0.5 \leq U_r \leq 1.0$ would be expected if the Strouhal number is based on the average of the velocities for the top and bottom of the plate.

A comparison of the previous vortex shedding experimental results with the lip noise data of references 1 and 2 indicates good agreement even though the test velocities differed by an order of magnitude. To illustrate, at a velocity ratio of unity the lip noise frequency in reference 1 was 20 000 Hz at a stream velocity of 244 m/sec and a lip thickness of 0.254 cm. For these conditions the Strouhal number was 0.21. The Strouhal number St is defined as

$$St = \frac{fh}{U}$$

where

f shedding frequency

h lip thickness

U stream velocity

In the present vortex shedding experiment the frequency was 375 Hz, the velocity was 24.4 m/sec, and the trailing edge thickness was 1.27 cm. For these conditions the Strouhal number is about 0.20.

As the velocity ratio was reduced below unity there was a slight reduction in frequency for both the data of reference 1 and the present results. This is consistent with the previous observation that the average velocity on both sides of the blunt trailing edge should be used in computing the frequency. In agreement with the present vortex shedding results, the lip noise data of reference shown in figure 1 indicates a cutoff in lip noise when the velocity ratio drops below 0.5.

THEORY

Abernathy and Kronauer (ref. 4) have shown that the vortex formation in the wake of blunt bodies can be explained by considering the nonlinear interaction of two infinite initially parallel vortex sheets in an inviscid incompressible fluid. In their analysis, the vortex sheets were represented by two rows of point vortices which were subjected to an initial disturbance. Flow patterns based on the calculated motion of the point vortices indicated that the vortices tended to cluster and form clouds resembling the Karman vortex street. In the Abernathy-Kronauer model, the mean flow velocities outside the vortex streets were equal. The present analysis represents an extension of the previous method in which the effect of unequal external mean velocities on vortex formation is considered.

The analytical model of two horizontal rows of point vortices which are separated by a distance h is depicted in figure 7. Initially, these rows are parallel, but then they are perturbed by a sinusoidal disturbance of wavelength a. The wave patterns assumed by the upper and lower rows of vortices for various free stream velocity ratios are calculated as a function of time. The numbers of point vortices per wavelength in the upper and lower rows are N^+ and N^-, respectively (note that hereinafter the superscripts $+$ and $-$ will be used to denote the upper and lower rows, respectively). The free stream velocities are adjusted so that U attains a value U_1, as $y \to +\infty$ and a value U_2 as $y \to -\infty$. In the region $-h/2 < y < h/2$, the mean velocity is zero. As in the Abernathy-Kronauer analysis, only antisymmetric disturbances (symmetric disturbances shifted by one-half wavelength in one of the sheets) will be considered, since these were shown in the previous reference to give the first indication of a vortex street arrangement.

The differential equations governing the motion of the vortex centers (x_j, y_j) of the individual point vortices in time are

$$\left.\begin{aligned} \frac{dx_j^{\pm}}{dt} &= u(x_j^{\pm}, y_j^{\pm}) \qquad (1) \\ \text{and} \qquad & \qquad (j = 1, 2, \ldots, N^{\pm}) \\ \frac{dy_j^{\pm}}{dt} &= v(x_j^{\pm}, y_j^{\pm}) \qquad (2) \end{aligned}\right\}$$

with $2(N^+ + N^-)$ unknowns $x_j^{\pm}(t)$ and $y_j^{\pm}(t)$. As in reference 4 an initial sinusoidal distribution of point vortices was imposed at zero time:

$$x_j^{\pm}(0) = \frac{(j-1)a}{N^{\pm}} \pm \frac{1}{4}a + A \sin\left[\frac{2\pi(j-1)}{N^{\pm}}\right] \qquad (3)$$

and

$$y_j^{\pm}(0) = \pm\frac{1}{2}h \bullet B \sin\left[\frac{2\pi(j-1)}{N^{\pm}}\right] \qquad (4)$$

where the constants A and B are associated with the initial disturbance.

The velocity components u and v of the individual vortex elements (eqs. (1) and (2)) are composed of an average velocity $\overline{U}$ due to the freestream motion as well as a velocity induced by all of the other vortex elements, that is,

$$u(x, y) = \overline{U} + \sum_{k=1}^{N^+} u_k^+(x, y) + \sum_{k=1}^{N^-} u_k^-(x, y) \qquad (5)$$

and

$$v(x, y) = \sum_{k=1}^{N^+} v_k^+(x, y) + \sum_{k=1}^{N^-} v_k^-(x, y) \qquad (6)$$

where

$$u_k^{\pm}(x, y) = \pm \frac{\overline{U}}{(N^+ + N^-)} \frac{\sinh\left[2\pi(y - y_k^{\pm})/a\right]}{\cosh\left[2\pi(y - y_k^{\pm})/a\right] - \cos\left[2\pi(x - x_k^{\pm})/a\right]} \tag{7}$$

$$v_k^{\pm}(x, y) = \mp \frac{\overline{U}}{(N^+ + N^-)} \frac{\sin\left[2\pi(x - x_k^{\pm})/a\right]}{\cosh\left[2\pi(y - y_k^{\pm})/a\right] - \cos\left[2\pi(x - x_k^{\pm})/a\right]} \tag{8}$$

$$(k = 1, 2, \ldots, N^{\pm})$$

Equations (1) to (8) are similar to those given in reference 4, but have been modified for unequal velocities over the top and bottom of the plate. The velocity $\overline{U}$ is defined as the average of the free stream velocities over the top and bottom of the plate in the absence of the vortex rows and can be expressed simply as

$$\overline{U} = \frac{U_1 + U_2}{2} \tag{9}$$

The relation between the number of vortex elements per wavelength and the velocity ratio U_r (where $U_r = (U_2/U_1)$) can be obtained by considering the limits of the u-component of velocity as $y \to \pm\infty$. Thus we have

$$\lim_{y \to +\infty} u(x, y) = U_1 = \frac{2N^+}{N^+ + N^-} \overline{U} \tag{10}$$

and

$$\lim_{y \to -\infty} u(x, y) = U_2 = \frac{2N^-}{N^+ + N^-} \overline{U} \tag{11}$$

or

$$U_r = \frac{U_2}{U_1} = \frac{N^-}{N^+} \tag{12}$$

Thus the ratio of vortex elements in the lower and upper rows is equal to the velocity ratio U_r. In the calculations the number of vortex elements per wavelength in the lower

row was held constant at $N^- = 21$ for all values of U_r. Obviously, as U_r decreases, the total number of vortex elements increases. For example, when $U_r = 0.25$, the number of vortex elements in the upper row is equal to four times the number in the lower row, that is, $N^+ = 84$. In this extreme case, the total number of differential equations (eqs. (1) and (2)) describing the motion of the vortex elements is 210 whereas at a velocity ratio of 1.0 the total number of differential equations is 84.

The solution of the system of differential equations was obtained by using a fourth-order Runge-Kutta method with a constant step size Δt which was chosen to be $0.056\ a/\overline{U}$. Although this step size is somewhat larger than the value used in the majority of the reference 4 calculations, it was adequate to provide good agreement with the published results for a velocity ratio of 1.0 (this can be noted by comparing fig. 8 with fig. 11 of ref. 4). This larger step size permitted the calculations to be made for a velocity ratio 0.25 (210 equations) within a practical computing time of about 25 minutes on an IBM 7094 upon limiting the nondimensional time $t\overline{U}/a$ to a value of about 2.25. In the nomenclature of reference 4 the value of $t\overline{U}/a$ corresponds to twice their value of tU/a (since $\overline{U}$ in the present model is equivalent to $2U$ in ref. 4).

All of the calculations were performed for a spacing ratio h/a of 0.281 (Karman ratio). The constants A and B, associated with the initial disturbance, had values of -0.0890 and -0.0749, respectively, as used in reference 4.

COMPARISON OF EXPERIMENT AND THEORY

The results of the previous calculations are shown in figures 8 to 11 as plots of the point vortex positions (x, y) at various times $t\overline{U}/a$ for values of velocity ratio U_r from 1.0 to 0.25. The periodic arrangement of point vortices, of which three oscillations are shown, is assumed to extend from $-\infty < x < +\infty$ at each instant of time. It should be noted that the actual vortex shedding phenomena of this experiment are not represented by these three oscillations, but rather by the changing point vortex patterns at increasing values of time, which can be seen by progressing downward in each figure. Thus the gradual accumulation of point vortices into clouds or clusters and their downstream movement with increasing time $t\overline{U}/a$ represent the experimental vortex shedding phenomena relevant to this investigation.

An examination of the theoretically computed vortex displacements as a function of time and velocity ratio in figures 8 to 11 show trends which agree in many respects with the experimental observations. First the results of these figures show that when the velocity ratio is reduced the rate of cloud formation in the lower row is also reduced and the clouds which form in the upper row become more and more diffuse. These diffuse regions of vorticity moving in random directions take on the appearance of random

turbulent motion much more than the more concentrated vortex clouds. This is consistent with the experimental observation that the vortex clouds become more indistinct as the velocity ratio was dropped, with the lower row disappearing faster than the upper.

The results for a velocity ratio of unity (fig. 8) show an equal tendency in the upper and lower vortex rows to roll up and form clusters or clouds of concentrated vorticity which form the characteristic elements of the classical Karman vortex street. A comparison of the velocity ratio unity results with other velocity ratios indicates a less rapid broadening of the wake as the velocity ratio is reduced for any given value of the nondimensional time parameters $t\overline{U}/a$. This result is in good agreement with the observations based on the smoke study photographs in figure 3.

Another observation concerns the increasing tendency of the lower clouds to fall behind and eventually be overtaken by the upper clouds. This same observation was made earlier in discussing the experimental results. Thus, there is no equilibrium position of the lower clouds relative to the upper for a velocity ratio other than unity, and the conventional steady symmetric vortex cloud spacing characteristic of the Karman vortex street is no longer possible. Apparently this lack of symmetry is responsible for the disappearance of the stable vortex cloud shedding frequency as noted in the experimental smoke studies and the coaxial nozzle noise studies of reference 1 as the velocity ratio was reduced.

In the earlier discussion of the smoke photographs convection velocities of the upper vortex street were measured. Likewise, convection velocities of vortex clouds can be inferred from the theoretical vortex patterns shown in figures 8 to 11. This was done by noting the x location of a given vortex cloud at each of the specified times and dividing the change of location by the time change. Establishing the location of a vortex cloud involved a judgment of which point vortices belong to a cloud and then assigning an approximate center to the cloud. Designating the upper vortex cloud velocity by V_1 and the lower by V_2, the measured velocities are shown in table II, together with those obtained from the movie film.

A comparison of the second and third columns indicates approximate agreement between experiment and theory for the ratio V_1/U_1, upper vortex cloud velocity to upper stream velocity. Because of the difficulty of determining vortex cloud centers from the smoke photographs, it was even more difficult to determine experimental vortex cloud velocities than it was for the theoretical vortex cloud developments of figures 8 to 11. Hence, a more exact agreement should not be expected.

The last column in table II is the ratio of the lower vortex cloud velocity V_2 to the upper cloud velocity V_1 as determined from figures 8 to 11. The excellent agreement between V_2/V_1 and U_2/U_1 for the first three cases indicates that the vortex clouds progress downstream at the same fraction of the free stream velocity for both the upper and lower vortex rows, that is $V_1/U_1 = V_2/U_2$.

The development of the vortex street for the $U_2/U_1 = 0.25$ case in figure 11 shows a much diminished tendency of the lower vortices to form well-defined clouds compared to the higher velocity ratios. Also an estimate of the ratio of what appears to be lower clouds to the upper cloud velocity V_2/V_1 is not necessarily the same as the ratio of the free streams U_2/U_1 as was the case for the larger velocity ratios. The values $V_2/V_1 = 0.23$ and 0.55 in table II are average values obtained for the two lower groupings of points which resemble loosely defined clouds.

CONCLUSIONS

An investigation was made of the vortices shed behind the blunt trailing edge of a flat plate. The ratio U_r of the free stream velocities on the two sides of the plate was varied from 1.0 to zero. The following observations were made:

1. Smoke study data indicated that the periodic vortex shedding which was evident at a velocity ratio of 1.0 tended to become less distinct and eventually disappeared as the velocity ratio U_2/U_1 approached zero where U_2 is lower free stream velocity and U_1 is upper free stream velocity. These observations provided an explanation for the phenomenon referred to as lip noise often observed in coaxial jets. The experiment showed that a Strouhal number of about 0.2, based on the lip thickness and a mean velocity $\overline{U}$, was associated with both vortex shedding and lip noise.

2. Theoretical calculations of the vortex formation based on an incompressible inviscid model of the vortex street were in good agreement with the experiment. The calculated wake flow patterns showed that, as the velocity ratio was reduced, there was less tendency to form clouds in the lower row (corresponding to the lower external mean velocity) and that the clouds in the upper row became more diffuse thus suggesting random turbulent motion. Also, as the velocity ratio approached unity, the clouds became more and more concentrated; this behavior was also verified by experiment.

Lewis Research Center,
National Aeronautics and Space Administration,
Cleveland, Ohio, April 7, 1975,
505-03.

REFERENCES

1. Olsen, W. A.; Gutierrez, O. A.; and Dorsch, R. G.: The Effect of Nozzle Inlet Shape, Lip Thickness, and Exit Shape and Size on Subsonic Jet Noise. AIAA Paper 73-187, Jan. 1973.

2. Olsen, W.; and Karchmer, A.: Lip Noise and Other Noise Generated by Flow Separation from Subsonic Nozzle Surfaces. Paper to be presented at American Institute of Aeronautics and Astronautics Meeting, Hampton, Va., Mar. 1975.

3. Herzig, H. A.; Hansen, A. G.; and Costello, G. R.: A Visualization Study of Secondary Flows in Cascades. NACA Rep. 1163, 1954.

4. Abernathy, F. H.; and Kronauer, R. E.: The Formation of Vortex Streets. J. Fluid Mech., vol. 13, pt. 1, May 1962, pp. 1-20.

5. Schlichting, Hermann: Boundary Layer Theory. McGraw-Hill Book Co., Inc., 1955.

TABLE I. - VORTEX SHEDDING FREQUENCIES

Velocity ratio, $U_r = U_2/U_1$	Hot wire measurements	Movie film measurements
	Shedding frequency, Hz	
1.0	370	375
.75	325	325
.5	320	320
.25	(a)	350
0	(a)	(a)

[a]None detected.

TABLE II. - RELATIVE VELOCITIES OF VORTEX CLOUDS

Free stream velocity ratio, $U_r = U_2/U_1$	Experimental velocity ratio, V_1/U_1 (using fig. 3 (smoke))	Analytical velocity ratio	
		V_1/U_1 (using figs. 5 to 8)	V_2/V_1 (using figs. 5 to 8)
1.0	0.71	0.70	1.0
.75	.59	.65	.78
.5	.59	.55	.48
.25	(a)	.50	0.23 - 0.55

[a]Undetectable.

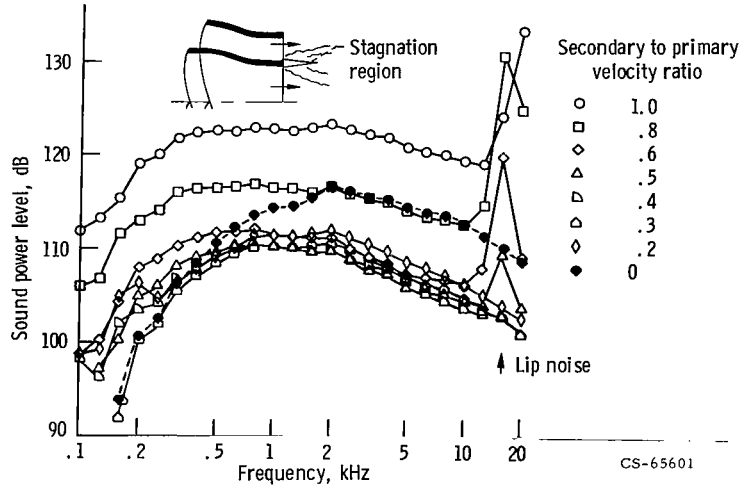

Figure 1. - Coaxial nozzle lip noise (ref. 1). Core velocity, 244 m/sec; core diameter, 5.28 cm; area ratio, 5.4; lip thickness, 0.25 cm; free field lossless data.

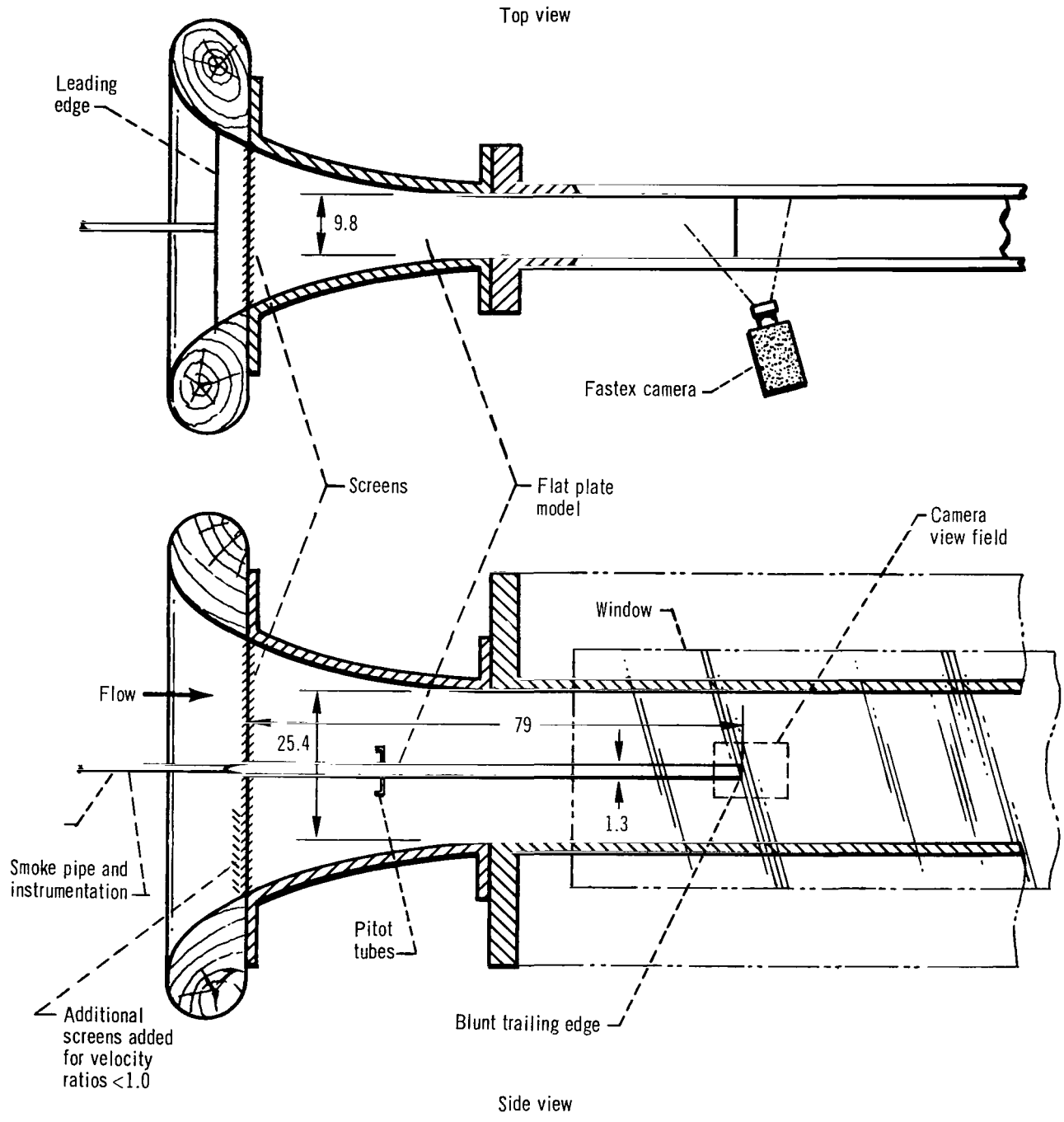

Figure 2. - Schematic diagram of wind tunnel with plate installed. (All dimensions in cm.)

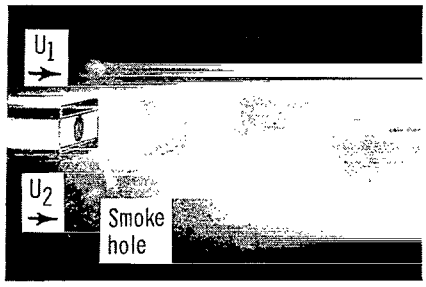

Magnification of one movie frame to show blunt trailing edge detail; $U_r = 1.0$. (X6)

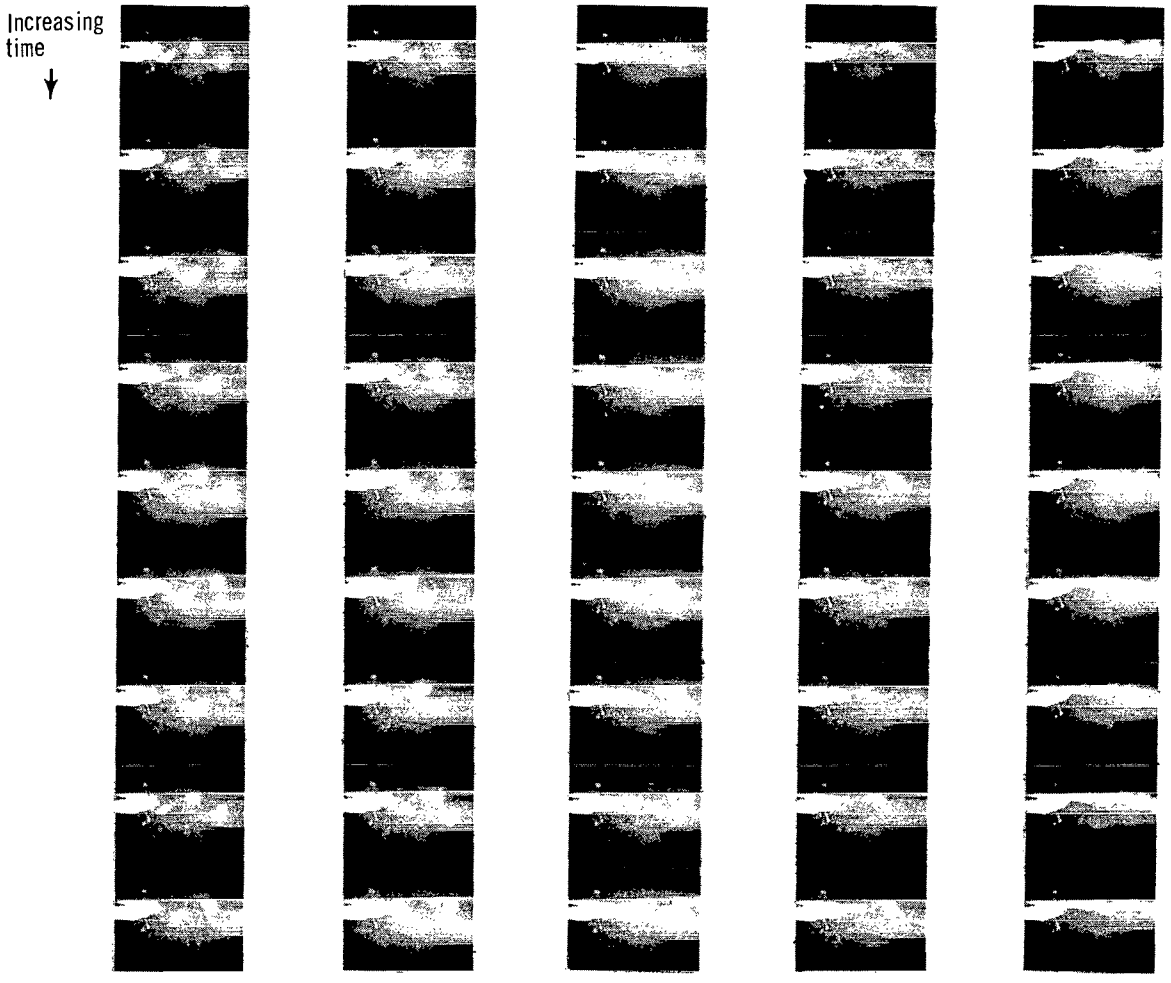

Direction of reduced vortex shedding →

(a) $U_r = 1.0$. (b) $U_r = 0.75$. (c) $U_r = 0.5$. (d) $U_r = 0.25$. (e) $U_r = 0$.

Figure 3. - Wake flow motion picture sequences at various velocity ratios ($U_r = U_2/U_1$). (X2)

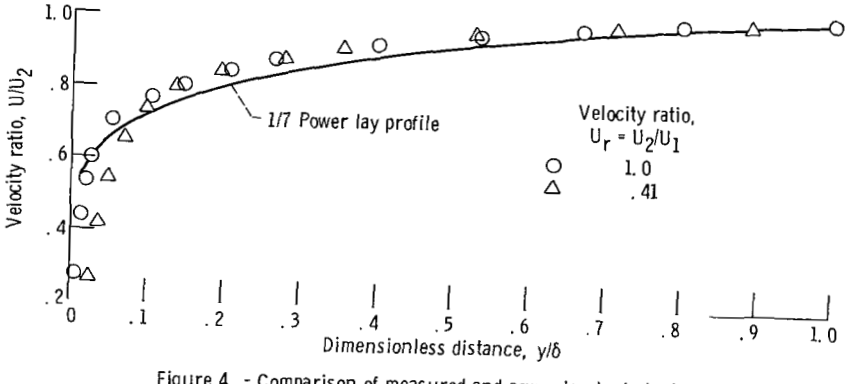

Figure 4. - Comparison of measured and power law turbulent profiles.

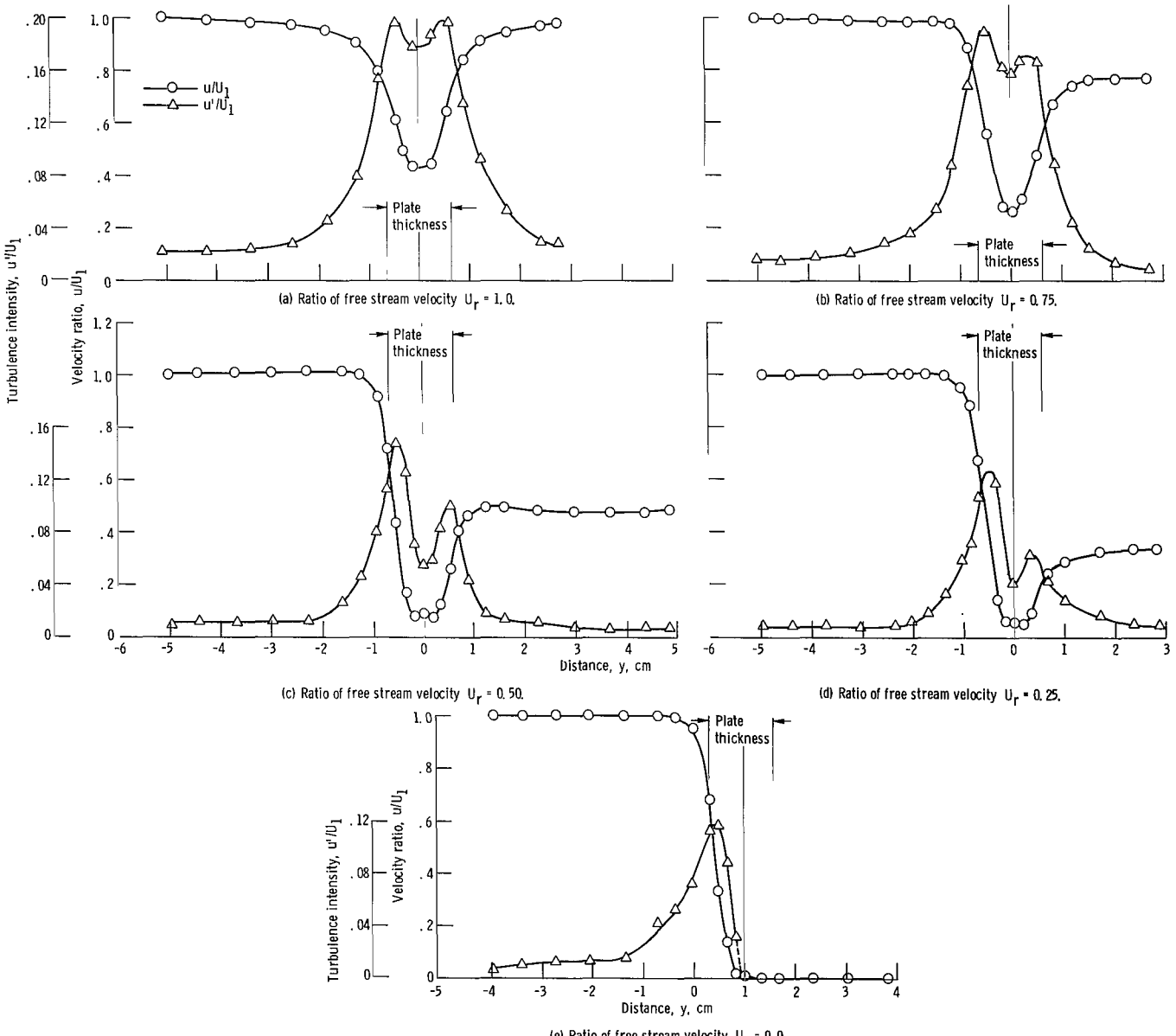

Figure 5. - Velocity and turbulence intensity profiles at X = 2.54 cm downstream of the trailing edge.

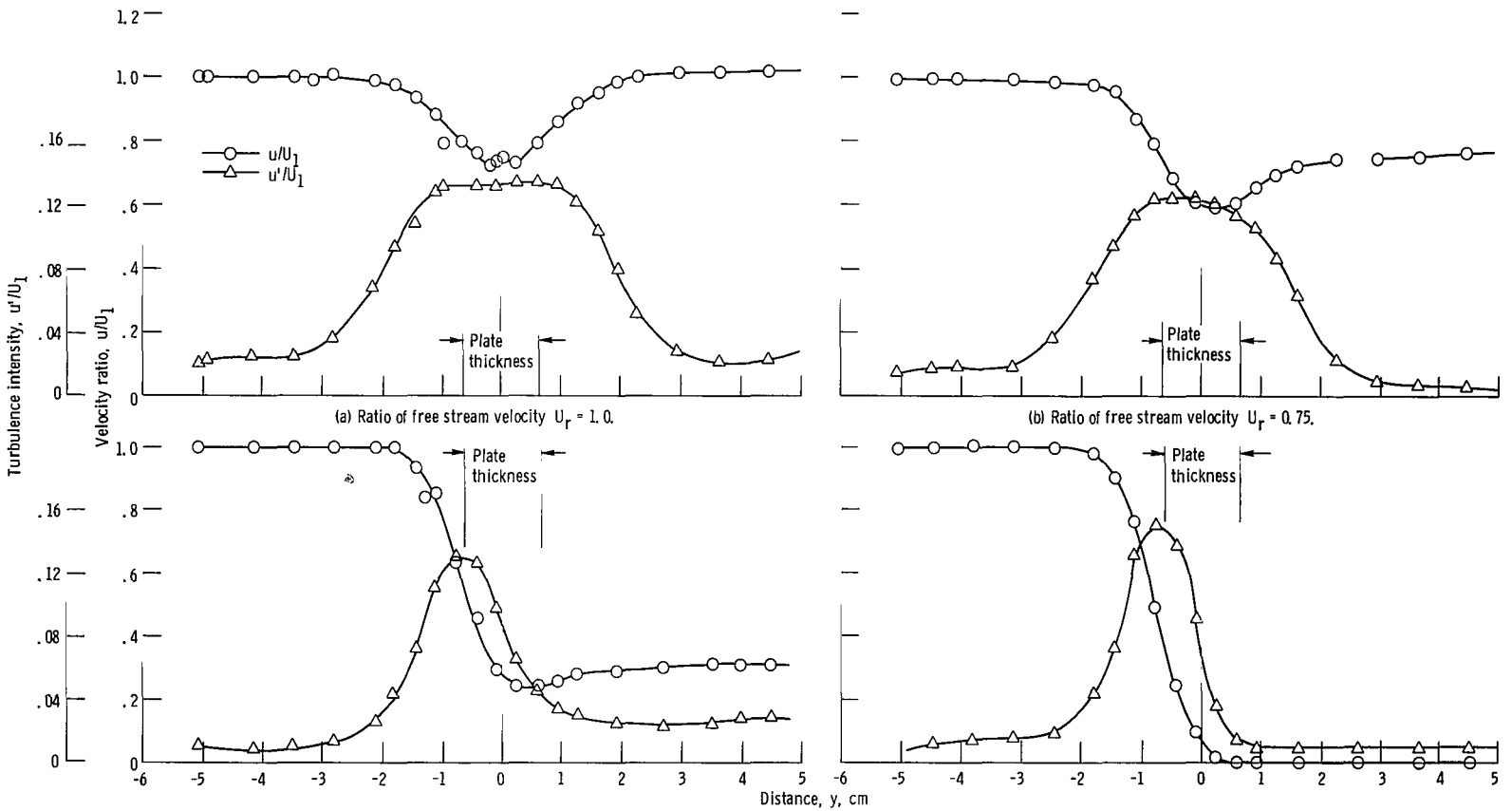

Figure 6. - Velocity and turbulence intensity profiles at x = 7.62 cm downstream of trailing edge.

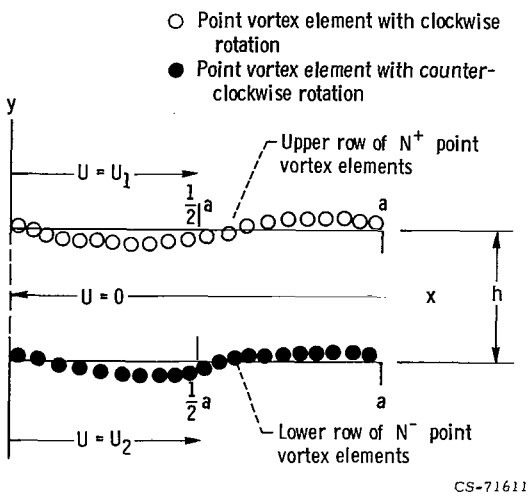

Figure 7. - One wavelength of a periodic perturbation of two initially parallel infinite vortex sheets.

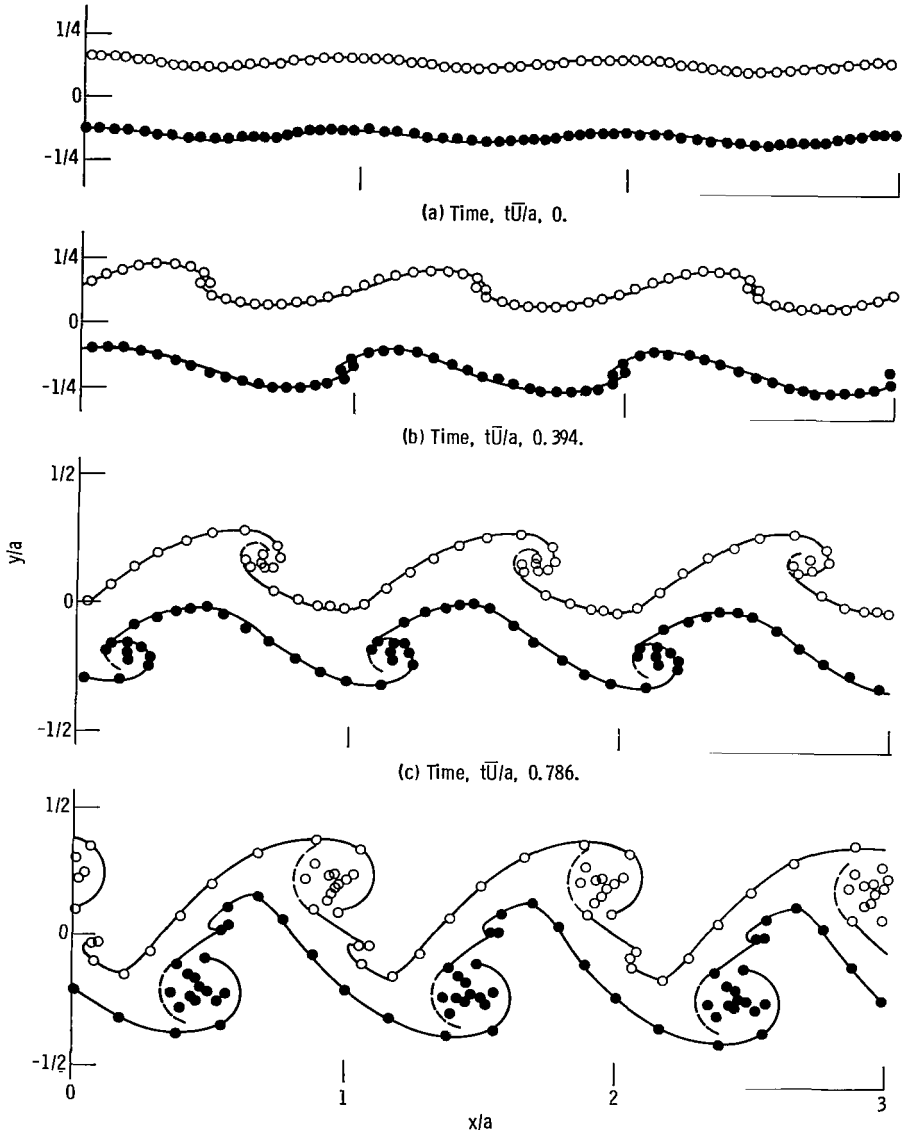

Figure 8. - Point vortex patterns at velocity ratio $U_r = 1.0$; $h/a = 0.281$; $\bar{U} = 1.0$; $A = -0.0890$; $B = -0.0749$; $N^+ = 21$; $N^- = 21$.

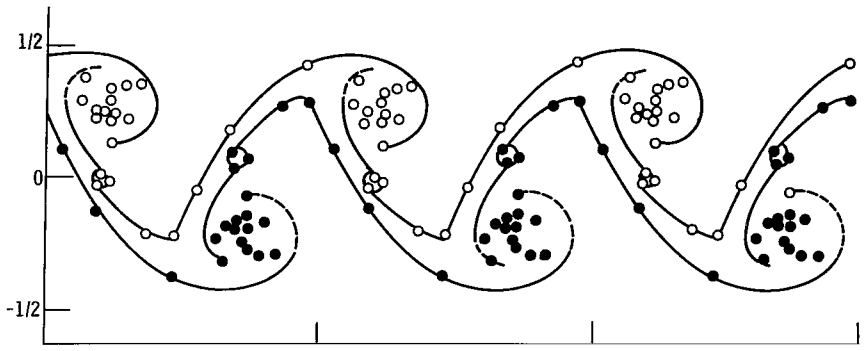

(e) Time, $t\bar{U}/a$, 1.573.

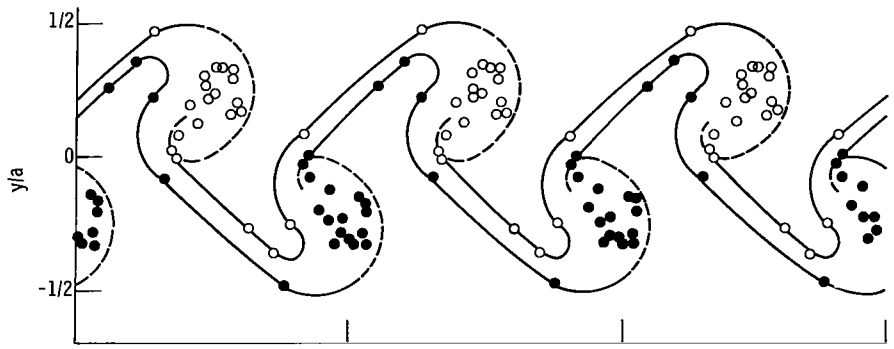

(f) Time, $t\bar{U}/a$, 1.910.

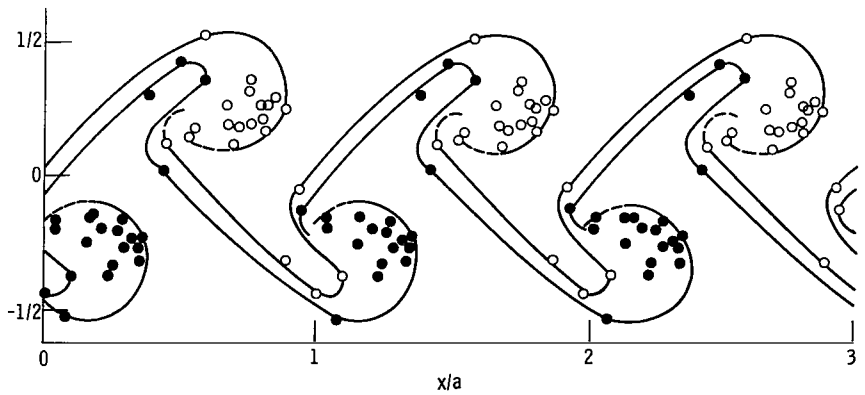

(g) Time, $t\bar{U}/a$, 2.248.

Figure 8. - Concluded.

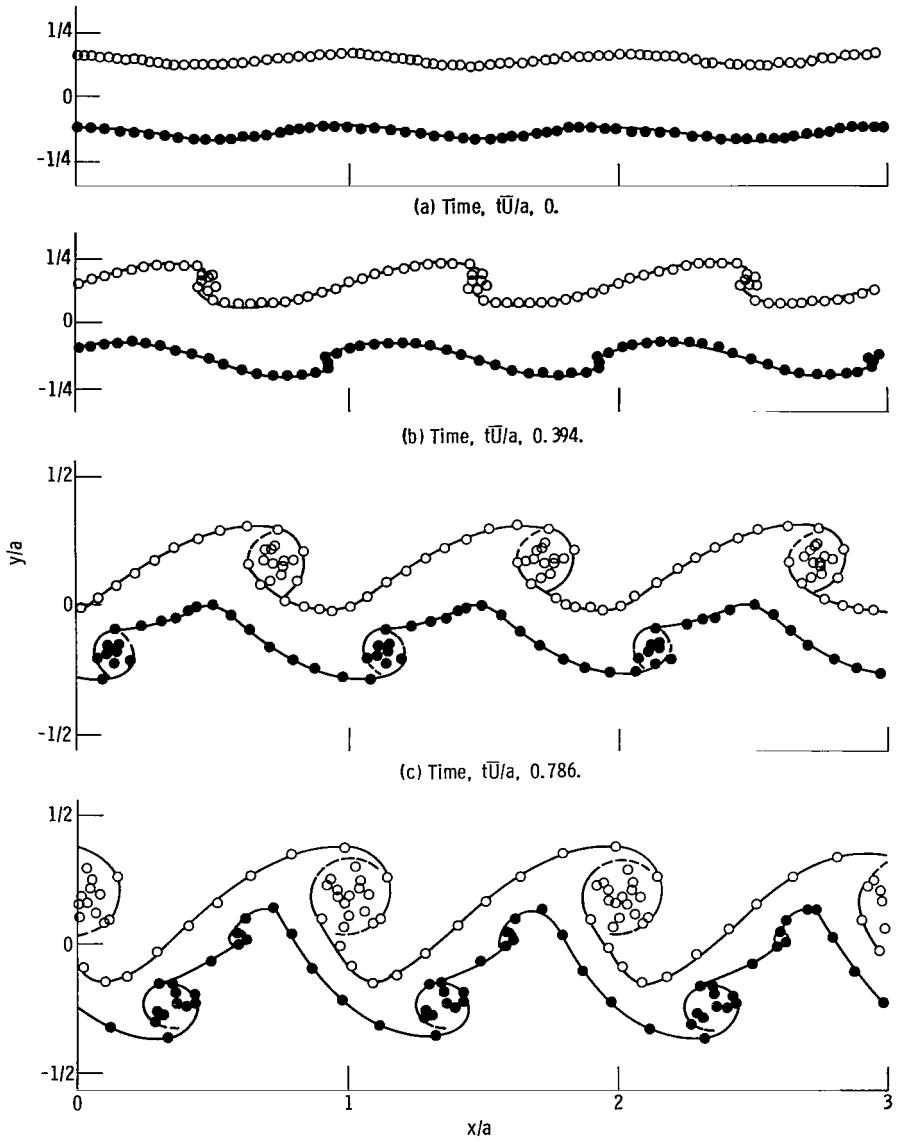

Figure 9. - Point vortex patterns at velocity ratio $U_r = 0.75$; $h/a = 0.281$; $\bar{U} = 1.0$; $A = -0.0890$; $B = -0.0749$; $N^+ = 28$; $N^- = 21$.

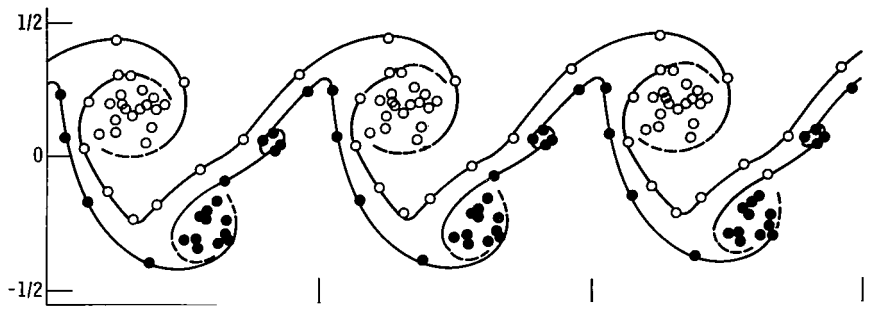

(e) Time, $t\bar{U}/a$, 1.573.

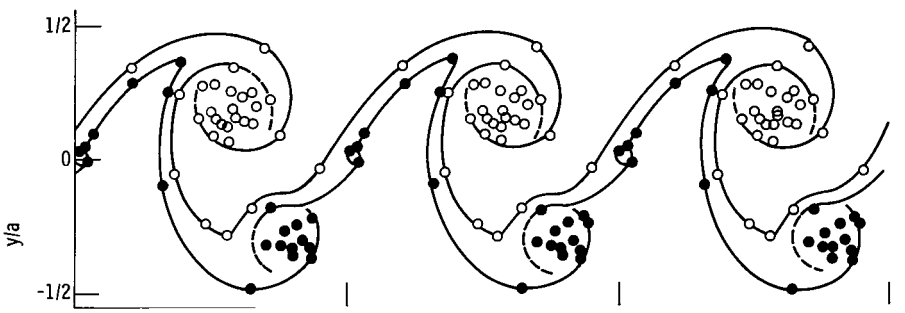

(f) Time, $t\bar{U}/a$, 1.910.

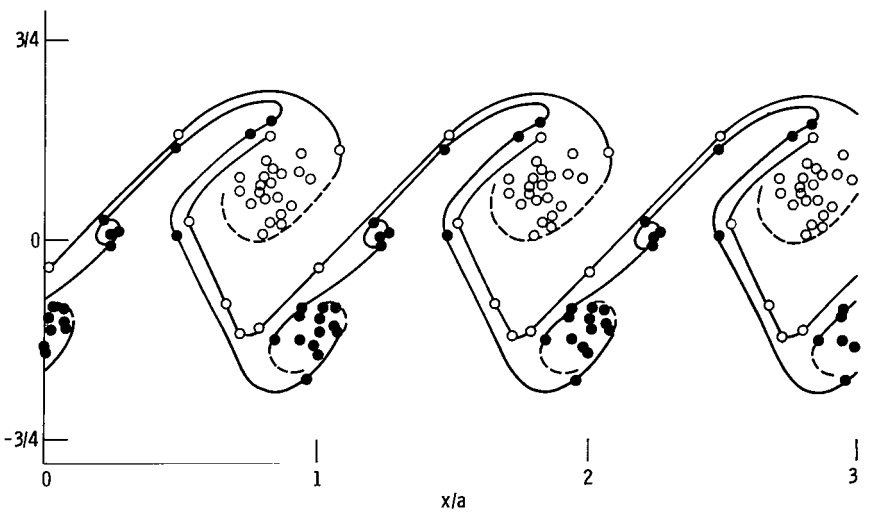

(g) Time, $t\bar{U}/a$, 2.248.

Figure 9. - Concluded.

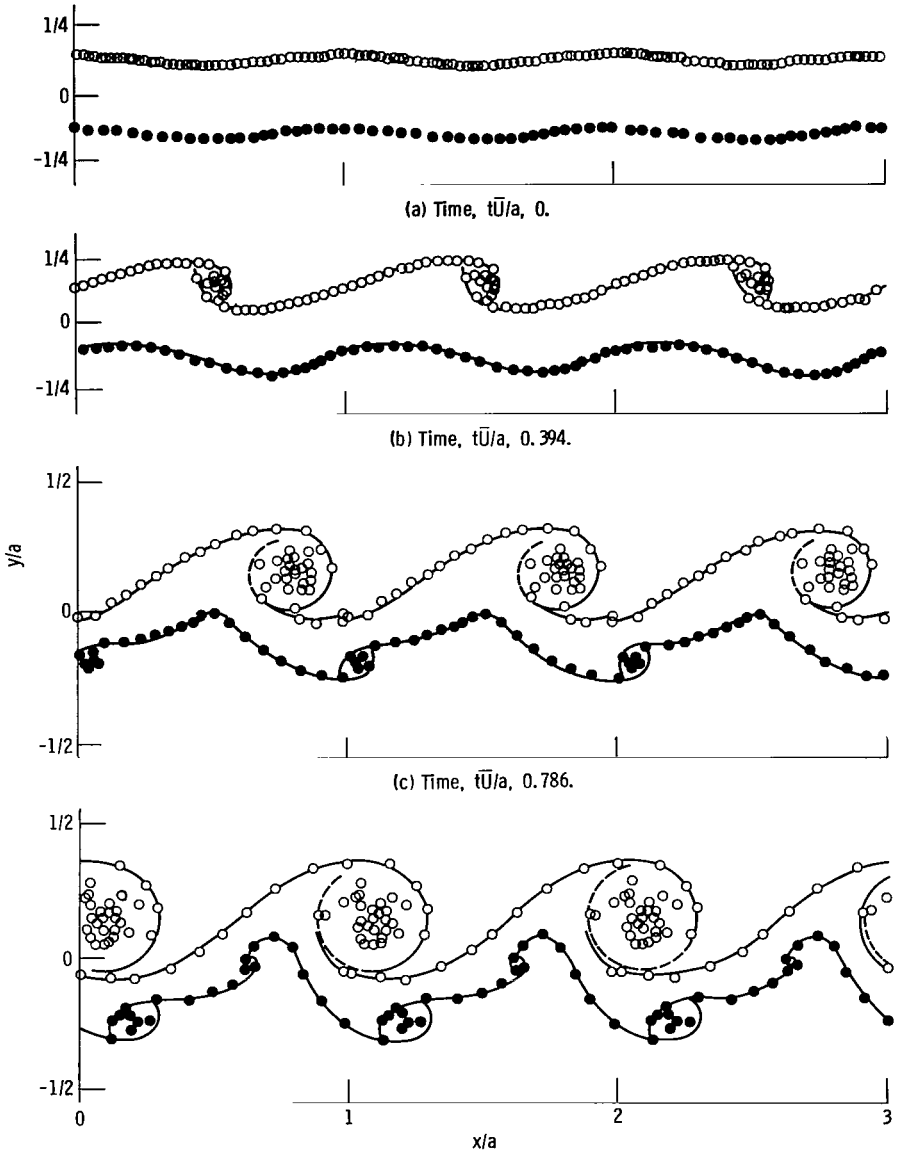

Figure 10. - Point vortex patterns at velocity ratio $U_r = 0.5$; $h/a = 0.281$; $\bar{U} = 1.0$; $A = -0.0890$; $B = -0.0749$; $N^+ = 42$; $N^- = 21$.

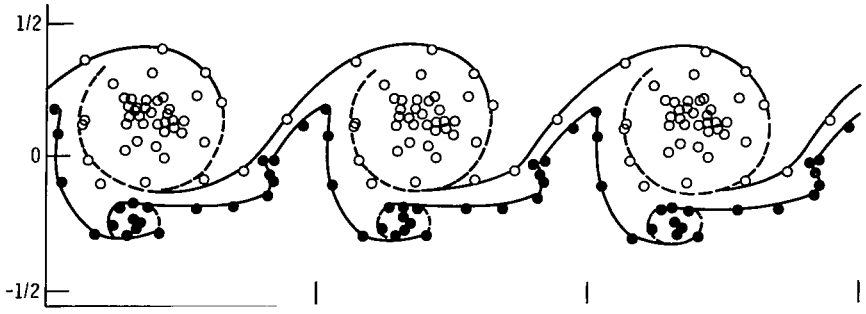

(e) Time, $t\bar{U}/a$, 1.573.

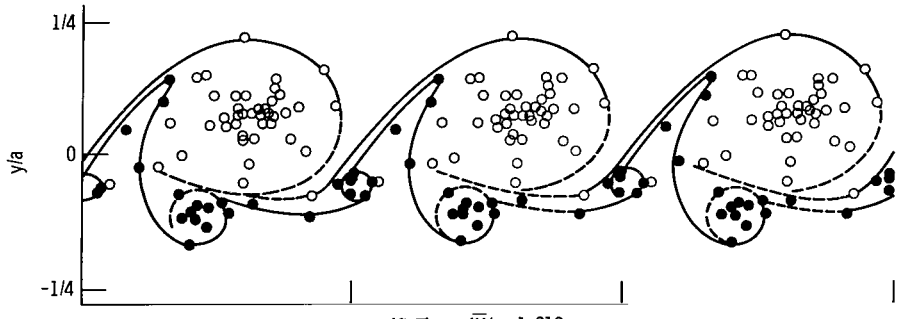

(f) Time, $t\bar{U}/a$, 1.910.

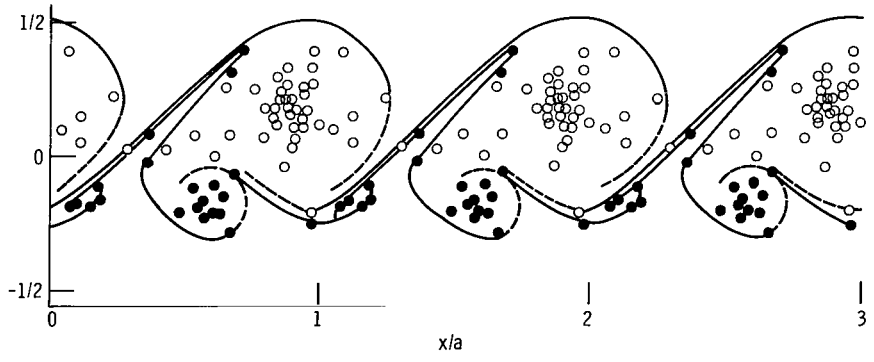

(g) Time, $t\bar{U}/a$, 2.248.

Figure 10. - Concluded.

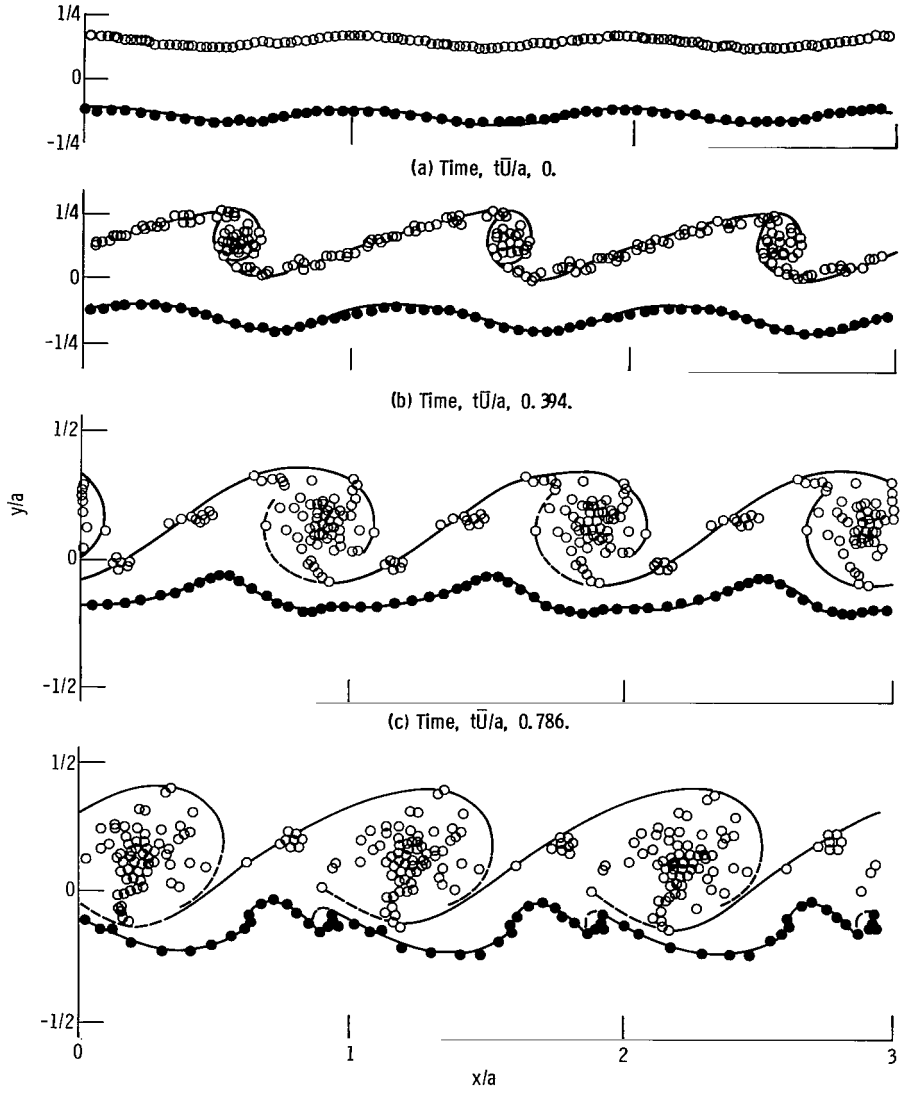

Figure 11. - Point vortex patterns at velocity ratio $U_r = 0.25$; $h/a = 0.281$; $\bar{U} = 1.0$; $A = -0.0890$; $B = -0.0749$; $N^+ = 84$; $N^- = 21$.

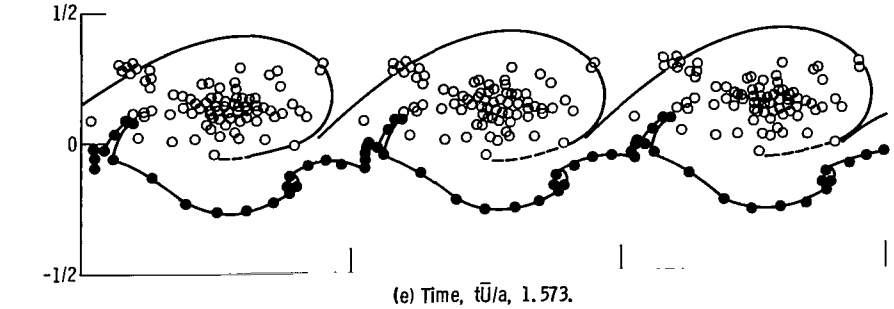

(e) Time, $t\bar{U}/a$, 1.573.

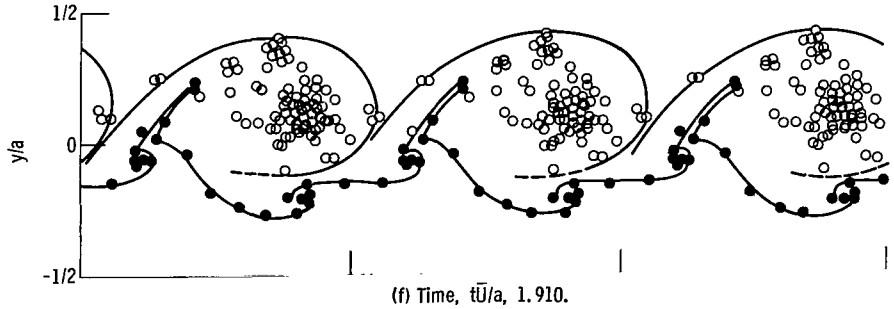

(f) Time, $t\bar{U}/a$, 1.910.

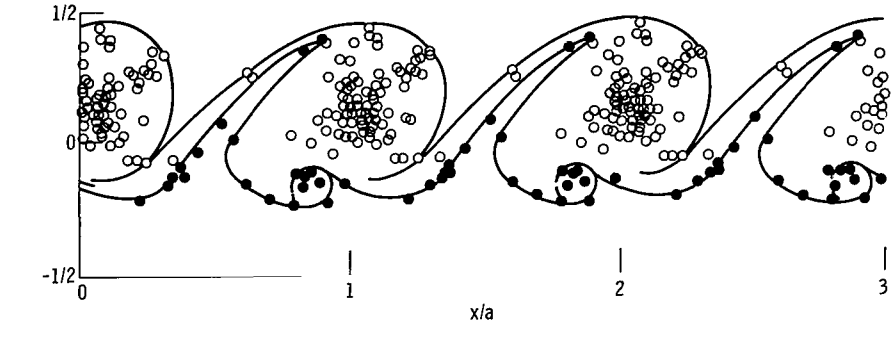

(g) Time, $t\bar{U}/a$, 2.248.

Figure 11. - Concluded.

NASA-Langley, 1975 E-8281

"The aeronautical and space activities of the United States shall be conducted so as to contribute . . . to the expansion of human knowledge of phenomena in the atmosphere and space. The Administration shall provide for the widest practicable and appropriate dissemination of information concerning its activities and the results thereof."

—NATIONAL AERONAUTICS AND SPACE ACT OF 1958

NASA SCIENTIFIC AND TECHNICAL PUBLICATIONS

TECHNICAL REPORTS: Scientific and technical information considered important, complete, and a lasting contribution to existing knowledge.

TECHNICAL NOTES: Information less broad in scope but nevertheless of importance as a contribution to existing knowledge.

TECHNICAL MEMORANDUMS: Information receiving limited distribution because of preliminary data, security classification, or other reasons. Also includes conference proceedings with either limited or unlimited distribution.

CONTRACTOR REPORTS: Scientific and technical information generated under a NASA contract or grant and considered an important contribution to existing knowledge.

TECHNICAL TRANSLATIONS: Information published in a foreign language considered to merit NASA distribution in English.

SPECIAL PUBLICATIONS: Information derived from or of value to NASA activities. Publications include final reports of major projects, monographs, data compilations, handbooks, sourcebooks, and special bibliographies.

TECHNOLOGY UTILIZATION PUBLICATIONS: Information on technology used by NASA that may be of particular interest in commercial and other non-aerospace applications. Publications include Tech Briefs, Technology Utilization Reports and Technology Surveys.

Details on the availability of these publications may be obtained from:

SCIENTIFIC AND TECHNICAL INFORMATION OFFICE

NATIONAL AERONAUTICS AND SPACE ADMINISTRATION

Washington, D.C. 20546